LDA Measurements and CFD Simulations of an In-Line High Shear Mixer with Ultrafine Teeth

Shuangqing Xu
School of Chemical Engineering and Technology, Tianjin University, Tianjin 300072, P.R. China

General Machinery Research Institute (GMRI), Hefei 230031, P.R. China

Qin Cheng
School of Chemical Engineering and Technology, Tianjin University, Tianjin 300072, P.R. China

School of Chemistry and Chemical Engineering, Anhui University, Hefei 230601, P.R. China

Wei Li, and Jinli Zhang
School of Chemical Engineering and Technology, Tianjin University, Tianjin 300072, P.R. China

DOI 10.1002/aic.14315
Published online December 19, 2013 in Wiley Online Library (wileyonlinelibrary.com)

Hydrodynamics of a pilot-scale in-line high shear mixer (HSM) with double rows of ultrafine rotor and stator teeth, including the velocity profiles and power consumptions, were measured using laser Doppler anemometry and a torque transducer, respectively. Computational fluid dynamics simulations were conducted using the standard k-ε turbulence model with first- and second-order accuracy and large eddy simulation (LES) with the standard Smagorinsky–Lilly subgrid scale model. Predictive capabilities of the different turbulence models and discretization schemes were assessed based on the experimental data. It is found that the current LES can predict accurately the flow patterns for the strongly rotating and locally anisotropic turbulent flows in the complex in-line HSM. The results obtained are fundamental to explore potential applications of the in-line teethed HSMs to intensify chemical reaction processes. © 2013 American Institute of Chemical Engineers *AIChE J*, 60: 1143–1155, 2014
Keywords: high shear mixer, laser Doppler anemometry, computational fluid dynamics, large eddy simulation, power consumption, flow pattern

Introduction

High shear mixers (HSMs), with the characteristics of high rotor tip speeds, high shear rates, and highly localized energy dissipation rates near the mixing head, have been widely utilized in the emulsification, suspension, and grinding processes in food, cosmetic, and chemical industries,[1–6] and have great potential to intensify chemical reactions with fast inherent reaction rates but relatively slow mass transfer.[7–10] Compared with batch HSMs, in-line teethed HSMs have the advantages of continuous operation, short residence time, and relatively high throughput. Practically, teethed HSMs with narrow rotor and stator slots are recommended by both engineers and equipment suppliers for fine dispersions and fast reactive mixing. The in-line HSMs with multiple rows of rotor and stator teeth are believed productive to overcome the defect of fluid bypassing in the single-row teethed units.[1,11,12] Patented chemical productions using in-line HSMs have been increasingly reported recently, among which the units with multiple rows of fine teeth are favored.[13–20] However, flow pattern analysis of the practical in-line HSMs has been so far rarely reported, although it is fundamental to process design, optimization, and scale-up.

Advanced noninvasive experimental techniques including laser Doppler anemometry (LDA) and particle image velocimetry have been used to study the flow characteristics in batch HSMs with typical configurations of a single rotor blade surrounded by a single screen.[21–23] While for in-line HSMs, the experimental flow measurements require specially manufactured volute with transparent front and/or circumference for laser beam access. To the best of our knowledge, Calabrese et al.[11] provided only one literature on the LDA measurements in a simplified prototype of a commercial IKA Works, Inc. in-line HSM containing a single row of coarse teeth (i.e., only 12 rotor teeth and 14 stator teeth).

Computational fluid dynamics (CFD) tools are becoming powerful and popular to conduct reactor design and diagnosis, as they are less restricted by the operating conditions, less time-consuming, and less costly. It is well-known that the accuracy of the CFD prediction depends greatly on the adopted turbulence models, the grid density, the near-wall treatment, and the discretization schemes. So far, the reported numerical simulations of the single-phase flow in

Additional Supporting Information may be found in the online version of this article.

Correspondence concerning this article should be addressed to J. Zhang at zhangjinli@tju.edu.cn.

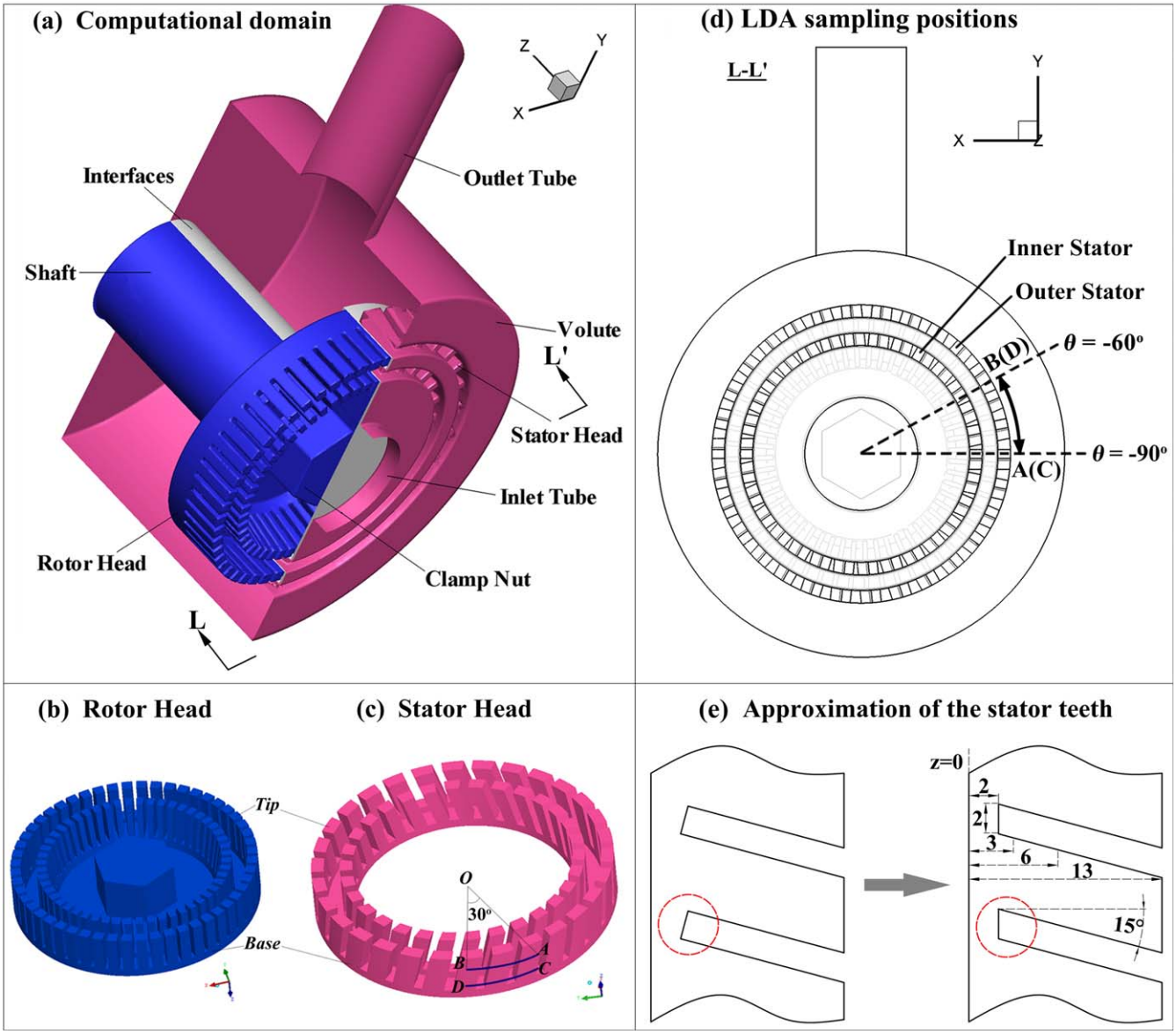

Figure 1. Computational domain in CFD and geometric details of the in-line HSM.

(a) Cutaway view of the computational domain consisting of a stationary part and a rotational part connected by predefined interfaces; enlarged views of (b) the rotor head and (c) the stator head; arcs AB and CD indicate the locations for LDA measurements; (d) front view of the mixer showing the LDA sampling positions for reference; (e) approximation of the stator teeth in the CFD model setup. [Color figure can be viewed in the online issue, which is available at wileyonlinelibrary.com.]

both batch and in-line HSMs adopted the standard k-ε turbulence model.[11,21,22,24] The accuracy of such CFD simulations still needs to be improved, owing to the inherent weakness of the standard k-ε turbulence model, for example, its unsatisfactory performance in the near-wall region, insensitivity to streamline curvature, and rotation as well as an unrealistic assumption of isotropic turbulence.[25,26] The large eddy simulation (LES), which has been successfully utilized to simulate complex flows in the stirred vessels,[27–33] turbomachineries,[34–37] and cyclones,[38–41] is a promising route to disclose more accurately the flow characteristics in the practical in-line HSMs.[10]

In this article, hydrodynamics of a pilot-scale in-line HSM with double rows of ultrafine rotor and stator teeth, including the velocity profiles and power consumptions, were first measured using LDA and a torque transducer, respectively. Then, the single-phase flow fields were estimated through CFD simulations using the standard k-ε modeling and LES. Predictive capabilities of the different turbulence models and discretization schemes were assessed based on the experimental data. It is found that the current LES can predict accurately the flow characteristics for the strongly rotating and locally anisotropic turbulent flows in the complex in-line HSM. The results obtained here are fundamental to explore potential applications of the in-line teethed HSMs to intensify chemical reaction processes.

Experimental Procedure

In-line HSM configuration

The experimental in-line HSM is a custom-built pilot-scale unit (FLUKO®, FDX1/60), of which the front and circumference of the volute as well as the stator were made from

Plexiglas. The transparent front volute was used for laser beam access in LDA measurements. The rotor consisted of two rows of 52 teeth (axially straight; with outer diameters of the inner and outer teeth rows of 47 and 59.5 mm) with 1-mm slots, whereas the stator had two rows of 30 teeth (15° backward inclined; with outer diameters of the inner and outer teeth rows of 53.5 and 66 mm) with 2-mm slots. The shear gap width (i.e., the annular space between the assembled rotor and stator) is 0.5 mm; and the tip-to-base clearance (i.e., the axial space from the rotor tip to the stator base, or that from the stator tip to the rotor base) is 1 mm. The inner diameter of the mixing chamber is 90 mm. Geometric details of the rotor and stator are shown in Figures 1b, c.

LDA measurements

The working fluid of pure water was fed to the in-line HSM by a centrifugal pump; therefore, the flow rate and rotational speed of the mixer were controlled separately. The inlet and outlet pressures of the mixer were almost equal to 1 atm monitored by the pressure gauges. The test temperature of water was controlled and monitored in the storage tank. In each run, the centrifugal pump and the mixer were turned on and operated under predefined conditions; while LDA acquisitions were activated only after the temperature in the tank became stable. In the LDA measurements, the rotational speed of the mixer varied from 1000 to 1600 rpm; whereas the volumetric flow rate ranged from 500 to 1000 L/h.

A two-component LDA system (Dantec Dynamics A/S) operated in back scattered mode was used to measure the radial and tangential velocities. The power of the laser transmitter (5 W Ar-ion system, Spectra Physics Laser) was kept at about 1 W in the measurements. The green and blue beams with the respective wavelengths of 514.5 and 488 nm were used. The focal length of the front lens was 310 mm. The beam spacing was 37 mm for the green and blue beams. The laser probe was mounted on a three-dimensional (3-D) computer-controlled traverse with minimum displacement of 0.01 mm in each direction.

The measurements were performed along two 30° arcs at different axial positions near the outer stator teeth (see arcs AB and CD in Figures 1c, d). Arc AB was near the half height of the stator teeth (corresponding to $z = 6$ mm in CFD), whereas arc CD was in the vicinity of the stator teeth base (corresponding to $z = 3$ mm in CFD). Each arc was meshed into 31 sampling positions with an interval of 1°. A large number of noncoincidence samples (10,000–40,000) were collected for each run and no data filtering was further applied. The velocity components at each position were presented as the ensemble average of instantaneous ones.

Measurement of power

Power consumption of the in-line HSM was measured by the torque method,[42–44] which was believed more accurate than the electric[45] or calorimetric method.[46,47] An AKC-215 transducer (China Academy of Aerospace Aerodynamics) was mounted on the drive shaft, from which the shaft torque and rotor speed of the mixer were recorded by a data-logging system at a frequency of 1 Hz. In the power consumption measurements, the rotor speeds were varied from 500 to 3500 rpm, while the flow rates were ranged from 500 to 2000 L/hr. The shaft bearing losses were measured and subtracted to obtain the net power consumption. The bearing losses were measured at zero flow rate by rotating the shaft at different rotor speeds without the rotor attached. The underlying assumption is that the power consumption by drag on the shaft is negligibly small comparing to the bearing loss.

CFD Simulations

Turbulence modeling

The standard k-ε model[48] is derived from the Reynolds-averaging of the underlying Navier–Stokes equations. The Boussinesq hypothesis is used to model the unknown Reynolds stresses by computing them as the product of the mean deformation rate and an isotropic turbulent viscosity. Two additional transport equations for the turbulence kinetic energy k and the turbulence dissipation rate ε are solved, and the turbulent viscosity is calculated as a function of k and ε. The standard k-ε model is essentially a high Reynolds number turbulence model assuming isotropic turbulence and spectral equilibrium.[25,26,33] The standard k-ε turbulence model is a popular Reynolds-Averaged Navier–Stokes model due to its robustness, economy, and reasonable accuracy for a range of turbulent flows.[26]

The governing equations for LES are obtained by filtering time-dependent Navier–Stokes equations. The filtering process effectively filters out eddies whose scales are smaller than the filter width or grid spacing used in the computations. The filtered equations, thus govern the dynamics of the large eddies; while the subgrid scale (SGS) stresses resulting from the filtering operation is modeled using an SGS model. The standard Smagorinsky–Lilly model, which is essentially an eddy-viscosity SGS model, relates the SGS stresses to the filtered variables through the adoption of the Boussinesq hypothesis. The underlying assumption is the local equilibrium between the transferred energy through the grid-filter scale and the dissipation of kinetic energy at small SGSs. Despite its simplicity and limitations, the standard Smagorinsky–Lilly model has the advantage of numerical robustness and stability.[28]

Mesh generation

As shown in Figure 1a, the 3-D computational domain consisted of two compartments (i.e., a stationary part and a rotational part) connected by the predefined interfaces. There were eight pairs of interfaces, four circumferential, and four transverse. An approximation of the stator teeth was made, as illustrated in Figure 1e, to facilitate model setup with better mesh quality. The clamp nut holding the rotor head was accounted for as it was relatively large and clearly influenced the flow field.

Unstructured tetrahedral elements were used for meshing. Good quality mesh with fine resolution was obtained using Gambit mesh generator. The computational domain of 3.49×10^{-4} m^3 was meshed into 1,941,911 cells, with over 50% cells located in the rotor-stator region. For both the standard k-ε modeling and LES, the inlet and outlet of the mixer were set as velocity inlet and pressure outlet boundaries. The inlet velocity was determined by the volumetric flow rate and the inner diameter of the inlet tube. The turbulence inlet conditions were specified by the turbulent intensity and the hydraulic diameter. The turbulent intensities, estimated by $I = 0.16\ (Re_D)^{-1/8}$, were 5.3 and 4.8% for the flow rates of

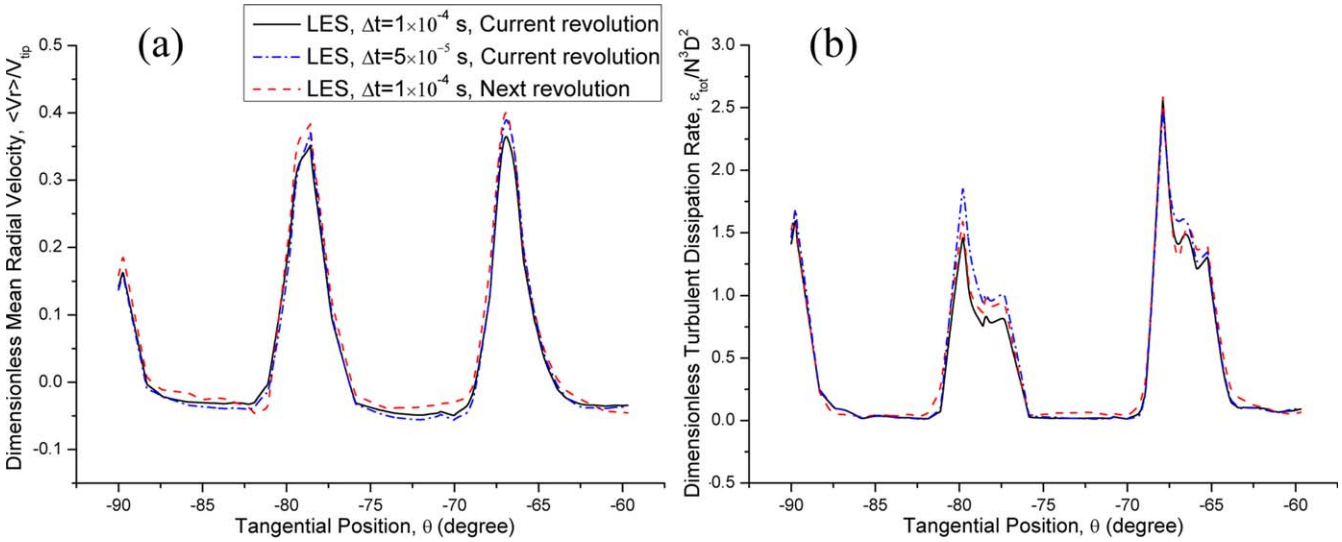

Figure 2. Effect of the time step size and elapsed calculation time on (a) the dimensionless mean radial velocity and (b) dimensionless turbulent dissipation rate at $z = 6$ mm, $r = 34$ mm predicted by LES for the case of $N = 1000$ rpm and $Q = 1000$ L/h.

[Color figure can be viewed in the online issue, which is available at wileyonlinelibrary.com.]

500 and 1000 L/h, respectively. The hydraulic diameter was set as the inner diameter of the inlet tube. In the case of LES, the spectral synthesizer method was chosen to model the fluctuating velocity at the velocity inlet boundary. No slip wall boundaries were applied to all the walls. Based on the calculated velocity gradients from the transient standard k-ε modeling with first-order accuracy and sliding mesh method, grid adaption to the original mesh was conducted. The locally refined grid contained 3,590,167 cells, with over 70% cells in the rotor-stator region. The cell volumes ranged from 5.158×10^{-13} to 6.476×10^{-10} m^3. Comparisons of the results from the standard k-ε model using both grid densities did not show significant differences, in term of the mean velocity profiles and the flow patterns. In the standard k-ε modeling of the three operating conditions, the global average $y+$ values are 0.67–1.05. Near the rotor-stator region where most of the mixing takes place, the average $y+$ values are 1.13–1.76. In the LES, the average $y+$ values are 0.60–0.89 in the whole computational domain and 1.04–1.51 near the rotor-stator region. In the case of LES, the length scales were resolved between 98 and 686 μm, which are of the typical order of the Taylor microscale of 80–320 μm and higher than the Kolmogorov's length scale of 10–21 μm (both estimated based on the average turbulent dissipation rates) in our study. This grid resolution can give realistic LES predictions.[33] In this article, all the CFD simulations were performed using the same refined computational mesh.

Solution methodology

CFD simulations were performed using commercial software Fluent. For the standard k-ε modeling with first-order accuracy, the first-order implicit unsteady formulation, as well as the first-order upwind scheme for momentum, turbulent kinetic energy, and turbulent dissipation rate was used. Whereas for the standard k-ε modeling with second-order accuracy, the second-order implicit unsteady formulation, as well as the second-order upwind scheme for momentum, turbulent kinetic energy, and turbulent dissipation rate was adopted. Enhanced wall treatment, which was reported to be able to describe flow in the viscous sublayer, buffer region, and fully turbulent outer region of the boundary layer,[21,22,24,26] was applied for both first- and second-order standard k-ε modeling. In the case of LES using the standard Smagorinsky–Lilly subgrid-scale model, the second-order implicit unsteady formulation and the bounded central differencing scheme for momentum was utilized. All the discretized equations were solved in a segregated manner with the semi-implicit method for pressure-linked equations algorithm. Standard model constants were used for all turbulence modeling.

In each case the problem was first solved using the first-order standard k-ε modeling, which was started with steady approximation using multiple reference frame technique in order to establish well developed time-averaged flow structure in the mixer. Then, the simulation was continued with the transient sliding mesh method to obtain a time-accurate solution for the rotor-stator interaction.[26] The converged results were used as the initial values for the second-order standard k-ε modeling and LES. In all simulations, the time period of a whole revolution Tr was divided into 600 time steps, corresponding to a time step size of Tr/600 and a resolution of 0.6° per time step. Taking the LES case of $N = 1000$ rpm and $Q = 1000$ L/h as an example, Figure 2 shows that further refinement of the time step size (i.e., to Tr/1200) gave little improvement to the results but increased significantly the time steps needed for a whole revolution. The results from the standard k-ε simulations utilizing the current time step size of Tr/600 (i.e., 1×10^{-4} s when $N = 1000$ rpm) and a larger one of 5×10^{-4} s are presented in Figure 3. There is little difference between the mean velocity profiles at $z = 3$ mm; whereas at $z = 6$ mm, little improvement can be observed by using a larger time step. When utilizing the current time step size of Tr/600, the global maximum Courant numbers are 3.4–4.7 for the standard k-ε modeling. The Courant number is a dimensionless number that compares the time step in a calculation to the

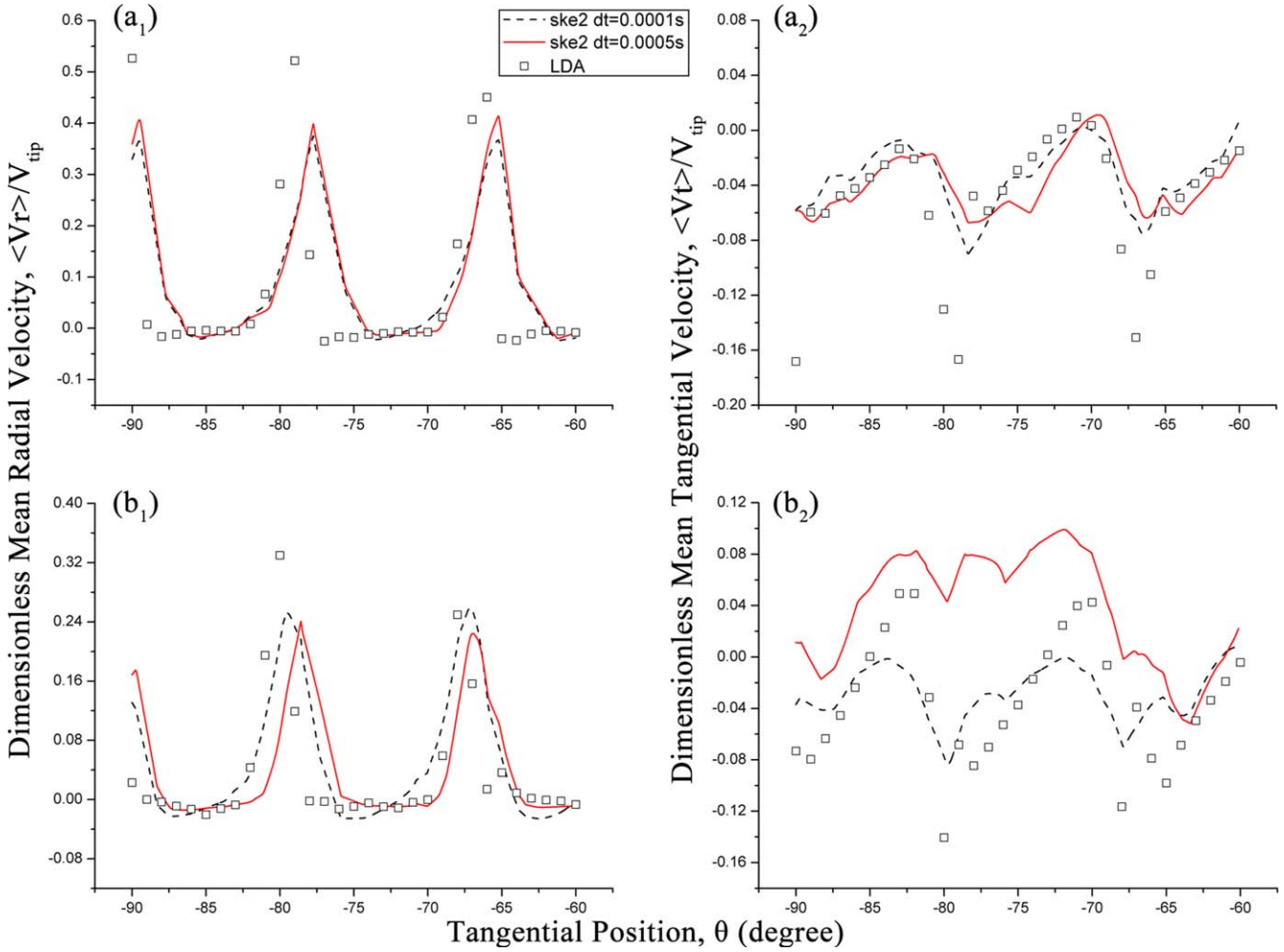

Figure 3. Effect of the time step size on the mean radial and tangential velocities predicted by the second-order standard k-ε modeling under $N = 1000$ rpm and $Q = 1000$ L/h at different axial positions: (a_1, a_2) $z = 3$ mm, $r = 34$ mm; (b_1, b_2) $z = 6$ mm, $r = 34$ mm.

[Color figure can be viewed in the online issue, which is available at wileyonlinelibrary.com.]

characteristic time of transit of a fluid element across a control volume (i.e., $u \cdot \Delta t/\Delta x$). For a stable, efficient calculation, the Courant number should not exceed a value of 20–40 in most sensitive transient regions of the domain.[26] For both the standard k-ε modelings and LES, utilizing large time step sizes (i.e., 0.001 s or larger) caused convergence difficulty and numerical instability. In all the CFD simulations, calculations were considered as converged when all the scaled absolute residuals decreased below 1×10^{-4}. The mass balance and the torque on the rotor were monitored to indicate convergence. The collection of transient data for time statistic analysis was started after the solution was fully converged, which took about 6–7 revolutions for the first-order standard k-ε modeling started with the initial result from the "coarse" computational mesh, and another 5–8 revolutions after switched to the second-order standard k-ε modeling and LES. Only one revolution of data was collected as repeat revolutions only produced repeat data.[25] Figure 2 also shows that the LES predicted results (under $N = 1000$ rpm and $Q = 1000$ L/h) demonstrate little differences between the data from the current and next revolution. In this study, all CFD simulations were performed using eight 2.26 GHz parallel processors with a total 12-GB memory. Typical calculation time per time step was about 160, 172, and 142 s for the first-, second-order standard k-ε modeling and LES, respectively.

Data Postprocessing

The measured and predicted velocity profiles were both angularly averaged, and expressed in a cylindrical coordinate system. The tangential and radial velocity components were normalized with the tip speeds based on the outer swept diameter of the rotor (i.e., 59.5 mm). This rotor outer swept diameter was also used for the calculations of the Reynolds numbers and flow numbers in this article.

The experimental and simulated power consumptions of the mixer were calculated as the product of the torque on the rotor and the angular velocity,[25,26,33] as shown in Eq. 1

$$P_{\text{fluid}} = 2\pi NT \tag{1}$$

where P_{fluid} is the net power delivered to fluid (W), N is the rotational speed (s^{-1}), T is the predicted torque in CFD simulations, or the net torque with bearing loss subtracted in the experiments (N m).

In LES, the turbulent dissipation rate ε was estimated as the contributions from both the resolved and SGS. By

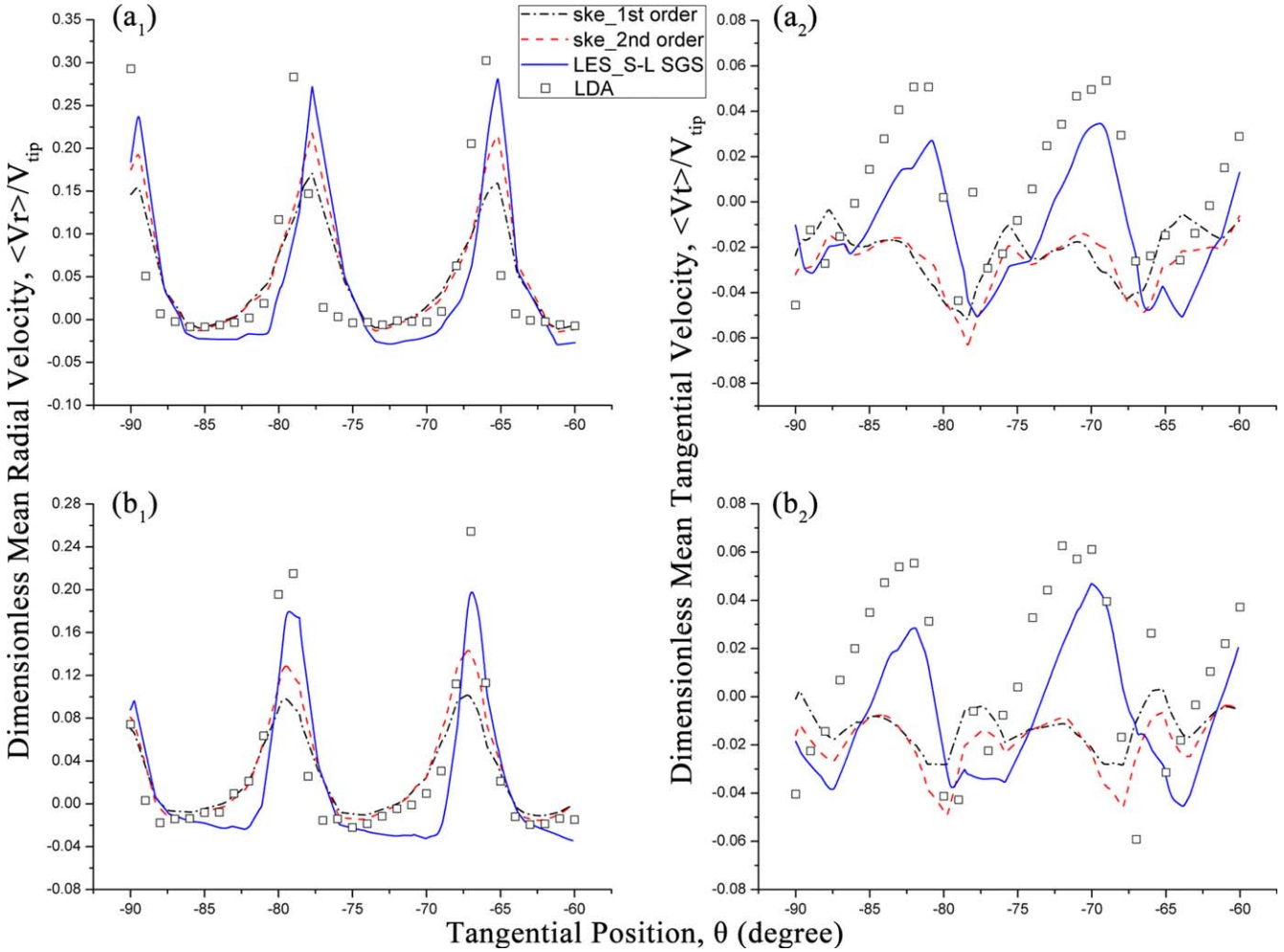

Figure 4. Comparison between the mean radial and tangential velocities from the LDA measurements and CFD simulations under $N = 1000$ rpm and $Q = 500$ L/h at different axial positions: (a_1, a_2) $z = 3$ mm, $r = 34$ mm; (b_1, b_2) $z = 6$ mm, $r = 34$ mm.

[Color figure can be viewed in the online issue, which is available at wileyonlinelibrary.com.]

assuming local equilibrium between the production and dissipation at and below SGS level, the energy dissipation rate at SGS was coupled to the deformation rate.[33,49] Then, the final expression for the turbulent dissipation rate was expressed as Eq.2[27,28,50]

$$\varepsilon_{tot} = \varepsilon_{res} + \varepsilon_{sgs} = \nu|S|^2 + (C_S\Delta)^2|S|^3 \quad (2)$$

where ε is the turbulent dissipation rate (m^2/s^3), ν is the kinematics viscosity (m^2/s), $|S|$ denotes the shear rate at the resolved scale (s^{-1}), Δ is the filter length (m), C_S is the Smagorinsky constant, adopting the default value of 0.1 which is typical in LES of shear-driven turbulent flows.

The LES predicted power consumptions can also be estimated by the integration of ε over the mixer volume[25,33] (see Eq. 3)

$$P_{fluid} = \iiint_V \rho\varepsilon dV \quad (3)$$

where P_{fluid} is the power consumption (W), ρ is the fluid density (kg/m^3), ε is the turbulent dissipation rate (m^2/s^3), and V represents the whole computational domain.

Results and Discussion

Mean velocity profiles

Figure 4–6 show the experimental and simulated velocity profiles at different axial positions in the jet flow region under different operating conditions. Generally, all the measured velocity components show a spatial periodicity of about 12°, consistent with the distribution of stator teeth. The jet velocities (i.e., radial components) reach the maximum in front of stator teeth slots, and decrease to the minimum in front of stator teeth walls. On the contrary, the tangential velocities reach the maximum in front of stator teeth walls, and decrease to the minimum in front of stator teeth slots. The measured and predicted maximum values of the mean radial velocities $<Vr>_{max}/V_{tip}$ are almost proportional to the flow rate under the constant rotor speed except for few LDA data points (Figure 4 vs. Figure 5), due to the constant open area of all outer stator slots. Conversely, the experimental and simulated $<Vr>_{max}/V_{tip}$ are almost in inverse proportion to the rotor speed under the constant flow rate despite few anomalous LDA data points (Figure 5 vs. Figure 6), suggesting that the absolute jet velocities are independent of the rotor speed.

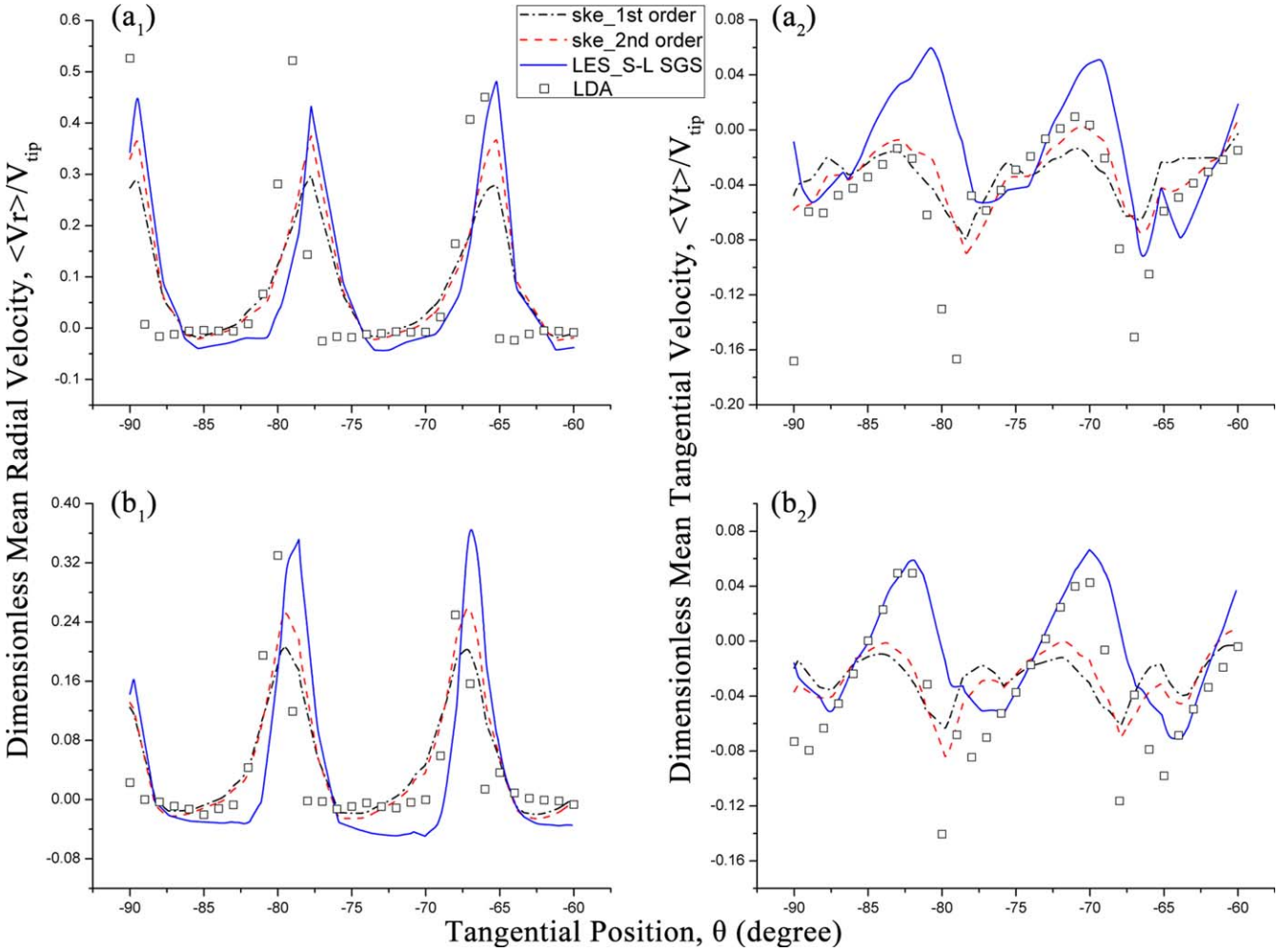

Figure 5. Comparison between the mean radial and tangential velocities from the LDA measurements and CFD simulations under $N = 1000$ rpm and $Q = 1000$ L/h at different axial positions: (a_1, a_2) $z = 3$ mm, $r = 34$ mm; (b_1, b_2) $z = 6$ mm, $r = 34$ mm.

[Color figure can be viewed in the online issue, which is available at wileyonlinelibrary.com.]

Predictive capability assessment

Compared with the LDA data, both the standard k-ε modeling and LES can predict the radial velocities with similar angular distributions and obvious periodicities. However, the first- and second-order standard k-ε modelings underestimate $<Vr>_{max}/V_{tip}$ with the errors even higher than 100%; whereas the LES predicted $<Vr>_{max}/V_{tip}$ values are much closer to the experimental results. As for the tangential components, the predictions from the first- and second-order standard k-ε modelings show less obvious periodicities as compared with LDA data. LES performs obviously better in terms of both the angular distributions and the maximum/minimum values. It is worth noting that LES can predict clockwise and counter clockwise tangential velocities of the approximate magnitude, which agree well with the LDA data. However, the predicted tangential velocities from the standard k-ε modeling are predominantly consistent with the rotational direction. In other words, LES is superior to capture the secondary flow characteristics in the jet flow region near the outer stator head. Using the same refined computational grid in our study, the first- and second-order standard k-ε modelings predict similar tangential velocity profiles; while for the radial velocities, an improvement in the prediction accuracy is achieved by the second-order standard k-ε modeling. The predictive performance of the standard k-ε model is generally better at $z = 3$ mm than that at $z = 6$ mm. Due to the inlet effect (i.e., proximity to the inlet tube) and the possible fluid bypassing through the slots, the jet velocities at $z = 3$ mm are nearly 1.5–1.7 times higher than those at $z = 6$ mm (see Figures 4–6). As the standard k-ε turbulence model is essentially a high Reynolds number model assuming fully turbulent flow,[26] this underperformance at $z = 6$ mm is probably due to the reduced turbulence and a deviation from the fully turbulent flow condition.

Among the different LES quality measures proposed in literature,[51] the one based on the viscosity ratio is utilized for the LES quality assessment in this article (see Eq. 4)

$$\mathrm{LESIQ}_v = \frac{1}{1+0.05\left(\frac{\langle v+v_t\rangle}{v}\right)^{0.53}} \tag{4}$$

where LESIQ_v is the index of LES quality (−), v and v_t are the kinematics and turbulent viscosities (m^2/s). It is reported that a LESIQ_v value greater than 80% is a good LES, and that over 95% approaches to a DNS. For the three operating conditions investigated in this article, the average LESIQ_v

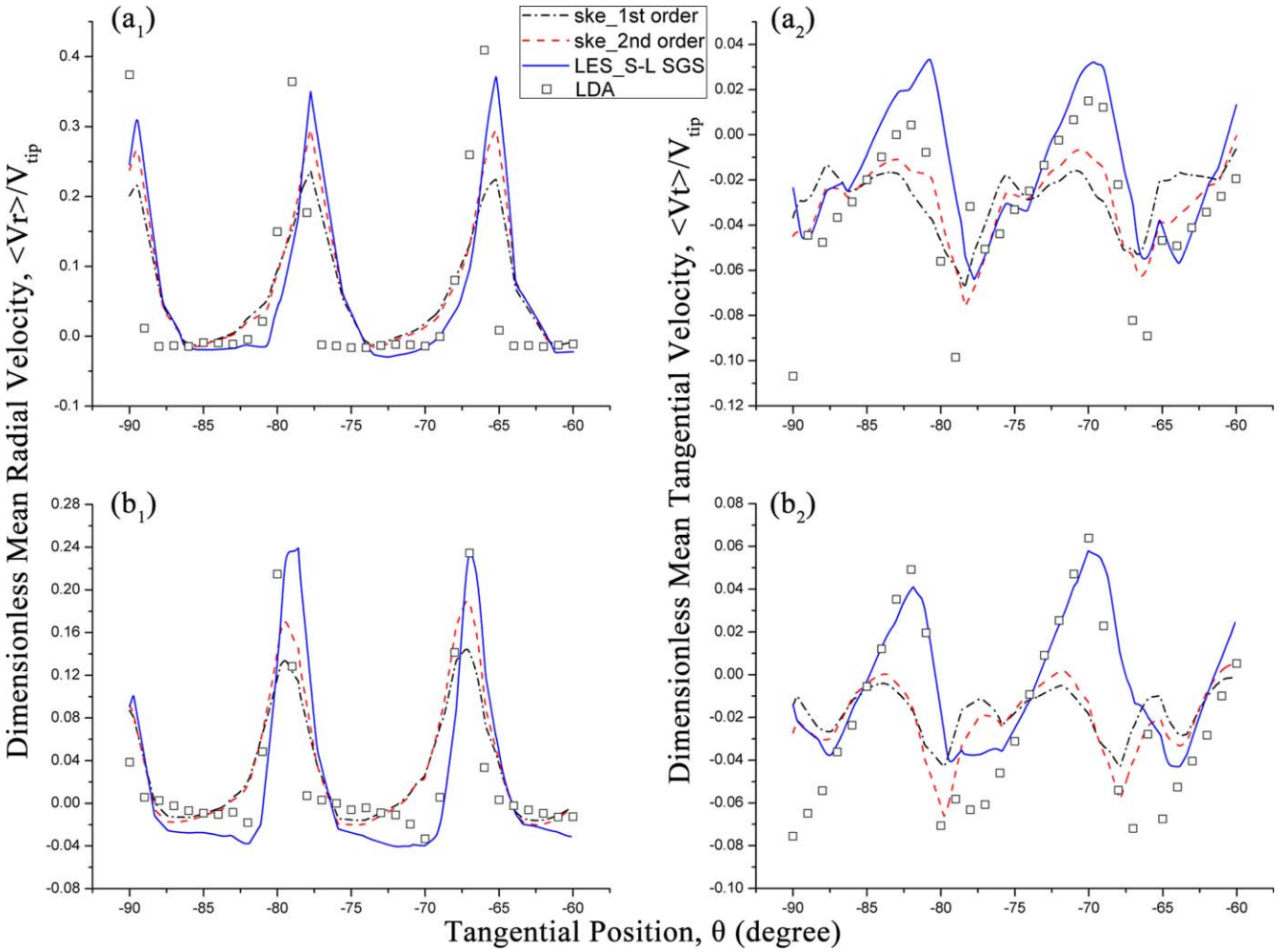

Figure 6. Comparison between the radial and tangential velocities from the LDA measurements and CFD simulations under $N = 1600$ rpm and $Q = 1000$ L/h at different axial positions: (a_1, a_2) $z = 3$ mm, $r = 34$ mm; (b_1, b_2) $z = 6$ mm, $r = 34$ mm.

[Color figure can be viewed in the online issue, which is available at wileyonlinelibrary.com.]

values are 93.0–93.7% in the whole computational domain and 92.1–93.1% near the rotor-stator region. The $LESIQ_v$ values above 80% indicate good performance of our LES.

Anisotropic analysis

To evaluate the level of local isotropy of turbulence inside the in-line HSM, the absolute differences between the different root mean square velocities were calculated based on the LES results and normalized by the rotor tip speed,[28,52,53] that is, $|u'-v'|/V_{tip}$ and $|w'-v'|/V_{tip}$. The turbulence is considered as isotropic when these values approximate zero. Figures 7a, b shows the contours of $|u'-v'|/V_{tip}$ and $|w'-v'|/V_{tip}$ on the plane of $z = 3$ mm for the case of $N = 1000$ rpm, $Q = 1000$ L/h. Enlarged view is used to show the details near the rotor-stator region and jet flow region. The corresponding results from $z = 6$ mm are not presented here for briefness but are alternatively provided as Supporting Information Figures S1 and S2. From Figure 7a, high values of $|u'-v'|/V_{tip}$ can be observed in the jet flow region near the outer stator, with a maximum of 0.162. The distribution of $|u'-v'|/V_{tip}$ is hardly influenced by the relative rotor position despite the little difference inside the inner rotor teeth slots. While high values of $|w'-v'|/V_{tip}$ exist inside the rotor teeth slots and the shear gaps (also near the clamp nut, results not shown here), with a maximum of 0.857 (see Figure 7b). The locally high values of $|u'-v'|/V_{tip}$ and $|w'-v'|/V_{tip}$ indicate the deviation from isotropic turbulence. Therefore, the standard k-ε model, based on the assumption of local isotropic turbulence, cannot provide accurate prediction for the flow in these regions.

LES predicted flow pattern

Taking the representative case of $N = 1000$ rpm and $Q = 1000$ L/h as an example, the LES predicted two-dimensional (2-D) velocity vectors at the upper right quadrant (including the LDA measured positions at $z = 3$ mm) are shown in Figure 8. As the flow is nearly stagnant away from the rotor-stator region and somewhat similar from one slot to the next, enlarged view is used to show the details around several rotor and stator teeth slots. The velocity vectors from $z = 6$ mm are provided as Supporting Information Figure S3. The flow pattern is rather complex as observed from Figure 8, including the jet, recirculation, and fluid re-entrainment, similar to those reported in both batch and in-line HSMs.[11,22,24,54] The fluid entering a stator slot (either inner or outer) impinges on the leading edge of the

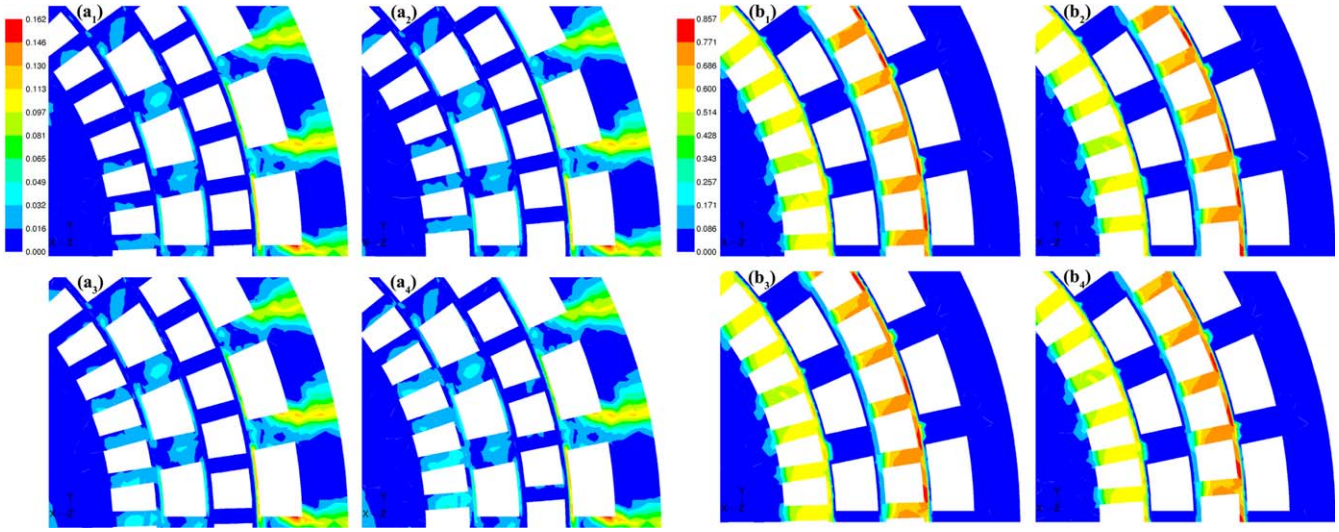

Figure 7. (a) Evolution of the LES predicted contours of $|u' - v'|/V_{tip}$ on the plane of $z = 3$ mm for the case of $N = 1000$ rpm and $Q = 1000$ L/h: (a_1) t; (a_2) $t + 5\Delta t$; (a_3) $t + 10\Delta t$; (a_4) $t + 15\Delta t$.

Enlarged view is used to show the details near the rotor-stator region and jet flow region. (b) Evolution of the LES predicted contours of $|w' - v'|/V_{tip}$ on the plane of $z = 3$ mm for the case of $N = 1000$ rpm and $Q = 1000$ L/h: (b_1) t; (b_2) $t + 5\Delta t$; (b_3) $t + 10\Delta t$; (b_4) $t + 15\Delta t$. [Color figure can be viewed in the online issue, which is available at wileyonlinelibrary.com.]

downstream stator tooth and emanating as a jet. The jet from the stator slot is always generated near the leading edge, while a circulation takes place near the trailing edge. The jet velocity generally shows symmetry from one stator slot to the next (as also indicated in Figures 4–6), due to the same open areas of all stator slots and the approximate flow rate through them as reported in literature.[11] Despite the periodicity of these overall characteristics, the flow field is influenced by the relative rotor position. The jet velocity increases as the rotor tooth approaches the leading edge of downstream stator tooth, reaches maximum when the rotor tooth begins to block the stator slot, and decreases as the rotor tooth moves away from the leading edge. Tangential velocities in the jet flow region near the outer stator are found periodically clockwise and counter clockwise along the tangential positions, consistent with the velocity profiles from Figures 4 to 6. This indicates that secondary flow characteristics are better captured by LES as compared with the standard k-ε modelings.

Figure 9 displays the LES predicted contours of the dimensionless turbulent dissipation rate ε/N^3D^2 on the plane of $z = 3$ mm for the case of $N = 1000$ rpm, $Q = 1000$ L/h. Enlarged view is used to show the details near the rotor-stator region and jet flow region. The corresponding results from $z = 6$ mm are provided as Supporting Information Figure S4. The logarithmic scale is used due to the large difference in magnitude. The large velocity gradients resulted from the fluid impingement and redirection as the rotor rotates rapidly lead to the high deformation rate and further high energy dissipation rate required for process intensification. That is why large values of ε/N^3D^2 are observed near the rotor-stator region and jet flow region, with a maximum of about 3000. The distribution of ε/N^3D^2 in the jet flow region is not so symmetrical from near one stator slot to the next. Although the geometric effect may exist (e.g., different proximity to exit), a major impact comes from the relative rotor position. The dissipation rate is highest in the nearest downstream stator slot relative to the rotor tooth and a little lower in the stator slots far away, as the fluid impingement and stagnation on the leading edge of the downstream stator teeth provides a major energy dissipation.[11,22,24] Within the stator teeth slots, ε/N^3D^2 is relatively small in magnitude at the positions where recirculation occurs.

The inhomogeneous nature of the turbulence level inside an in-line HSM should be taken into well consideration in the process design, optimization, and scale-up. When the single-pass operation mode is utilized (rather than the semi-batch mode where the in-line HSM functions in the recirculation loop downstream of a holding tank), the inhomogeneous turbulence together with the short residence time can result in bimodal particle-size distribution in dispersion processes and/or undesirable byproducts in competing reaction processes. This influence on the final product may not be so significant when the materials are easy to disperse (or mix) and noncoalescing, but can be pronounced otherwise.

Power consumption

Power consumption, which is important for the performance assessment and motor selection of an in-line HSM, was measured by the torque method under a range of rotational speeds and volumetric flow rates. As LES gives better prediction of the flow pattern than the standard k-ε modeling, it was further used for the power consumption estimation under each operating condition.

The experimental and LES predicted power consumptions by the torque method are presented in Figure 10, indicating an increase with the rotor speed and flow rate. Power law fits between the power consumption and the rotor speed for both the simulated and measured results give indexes near 2, consistent with those from Sparks.[44] The LES predicted power consumptions by the torque method show good agreement with the experimental data, with an overall average error of 20.4%. Under the flow rates above 500 L/h, the average error between the measured and simulated power consumptions is only 14.9%, although there is a deviation

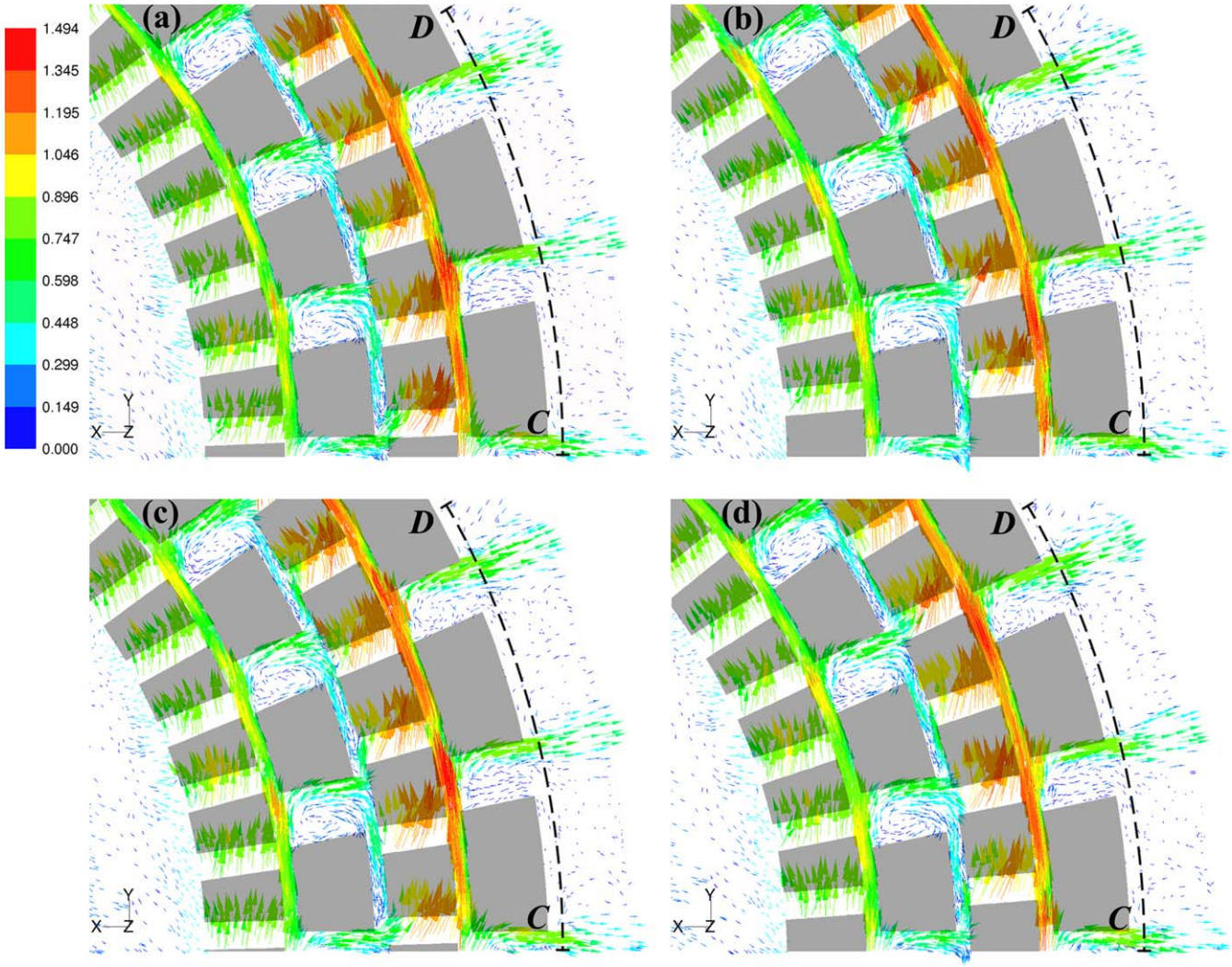

Figure 8. Evolution of the LES predicted 2-D velocity vectors on the plane of $z = 3$ mm colored by the dimensionless velocity magnitudes for the case of $N = 1000$ rpm and $Q = 1000$ L/h: (a) t; (b) $t + 5\Delta t$; (c) $t + 10\Delta t$; (d) $t + 15\Delta t$.

Arc CD indicate the locations of the LDA measured positions. [Color figure can be viewed in the online issue, which is available at wileyonlinelibrary.com.]

under higher rotor speeds when operated at the lowest flow rate of 500 L/h.

Kowalski[45] proposed that the net power delivered to fluid by an in-line HSM consisted of: (1) the power required to rotate the rotor against the liquid (tank term) and (2) the power requirements from the flow of fluid (flow term). The "tank term" is analogous to the power consumption in a stirred vessel, whereas the "flow term" accounts for the pumping action of the in-line mixer. This power consumption model has been validated by the experimentations.[42,43,46,47,55]

The flow is considered as turbulent for the Reynolds numbers ranging from 2.8×10^4 to 2×10^5 in this article. Data regressions were then conducted using Kowalski's power consumption model[42] (as shown in Eq. 5), in order to obtain model constants for the power requirement estimations for given fluid properties, rotor dimensions, and operation parameters

$$Po = Po_{z(t)} + k_1 \mathrm{Fl} \tag{5}$$

where Po is the power number defined as $P_{\mathrm{fluid}}/\rho N^3 D^5$, Fl is the flow number defined as Q/ND^3, $Po_{z(t)}$ is the turbulent power number at zero flow rate, and k_1 is a model constant. Correlating the experimental power data with Eq. 5 gives $Po_{z(t)} = 0.147$ and $k_1 = 14.490$, with a R^2 value of 0.9100. Conversely, data regression using the LES results from the torque method yields $Po_{z(t)} = 0.139$ and $k_1 = 14.029$, with a R^2 value of 0.9969. Therefore, the method based on the LES predicted torque can accurately estimate the power consumption of the ultrafine teethed in-line HSM.

The turbulent power number at zero flow rate $Po_{z(t)}$ of 0.139–0.147 for the ultrafine teethed in-line HSM is very close to 0.145 for the Silverson 150/250 MS in-line mixer fitted with dual fine screens. Whereas the k_1 value of 14.029–14.490 is much higher than 8.79 for the dual fine Silverson,[43] indicating a more significant dependence of the power consumption on the processing flow rate for the ultrafine teethed unit. Under the fully turbulent regime with the same flow number, the ultrafine teethed HSM draws over 60% higher power than the dual fine Silverson.

The accuracy of the LES predicted ε is assessed by establishing energy balance, that is, by comparing the volume integration of ε with the experimental power consumption[33] (see Eq. 3). The LES predicted power consumptions by the

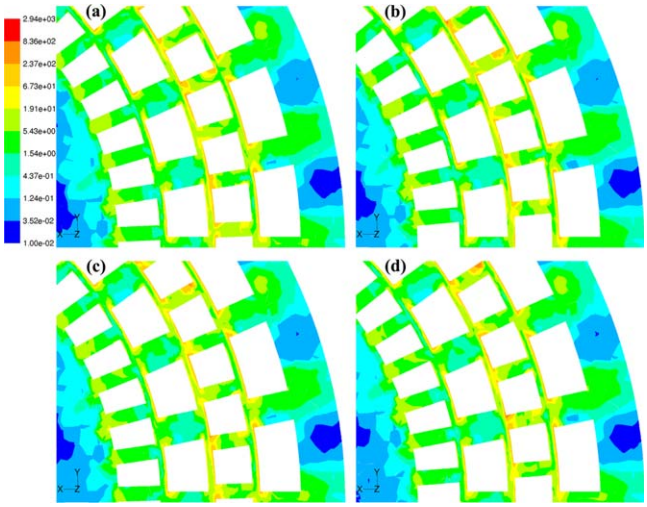

Figure 9. Evolution of the LES predicted contours of dimensionless turbulent dissipation rate ε/N^3D^2 on the plane of $z = 3$ mm for the case of $N = 1000$ rpm and $Q = 1000$ L/h: (a) t; (b) $t + 5\Delta t$; (c) $t + 10\Delta t$; (d) $t + 15\Delta t$.

[Color figure can be viewed in the online issue, which is available at wileyonlinelibrary.com.]

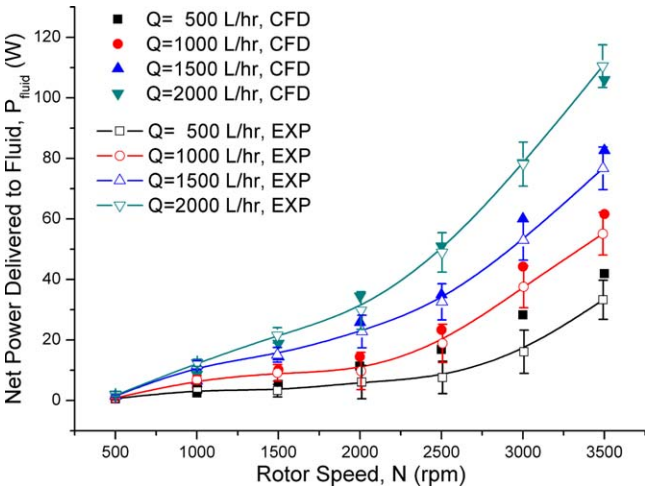

Figure 10. Comparison between the experimental and LES predicted power consumptions by the torque method under different rotor speeds and volumetric flow rates.

[Color figure can be viewed in the online issue, which is available at wileyonlinelibrary.com.]

integral ε method generally agree well with the experimental data at lower flow rates of $Q \leq 1000$ L/h, with an average error of 23.6%. This indicates the good prediction accuracy of ε in our LES within these operating conditions. It should be also noted that, the discrepancy becomes larger for $Q \geq 1500$ L/h, especially when $N \geq 3000$ rpm. This is probably caused by the universal Smagorinsky–Lilly SGS model constant used in all the simulations (i.e., $C_s = 0.1$). Other SGS models, such as the dynamic Smagorinsky–Lilly or dynamic kinetic energy SGS models, do not have such shortcomings and are worth testing in future investigations.

Conclusions

Single-phase flow fields and power consumptions were measured in a pilot-scale in-line HSM with double rows of ultrafine rotor-stator teeth. CFD simulations were conducted using the standard k-ε turbulence model with first- and second-order accuracy, and LES with the standard Smagorinsky–Lilly SGS model. Predictive capabilities of the different turbulence models and discretization schemes were assessed based on the experimental data. Both the measured and predicted velocities demonstrate a spatial periodicity of 12° in the jet flow region of the mixer, consistent with the distribution of the stator teeth. The maximum of the dimensionless mean radial velocities are almost proportional to the volumetric flow rates, and are almost in inverse proportion to the rotational speeds. The power consumption of the dual rows ultrafine teethed HSM shows more significant dependence on the flow rate than the dual fine Silverson unit of the similar scale. In the high Reynolds number turbulent regime with the same flow number, the ultrafine teethed HSM draws over 60% higher power than the dual rows Silverson with fine screen. Estimated power consumptions of the mixer based on the LES predicted torque agree well with the experimental data. LES can predict accurately the flow patterns for the strongly rotating and locally anisotropic turbulent flows in the complex in-line HSM. Other SGS models are worth being assessed in future in order to obtain good LES accuracy for a wide range of operating conditions. The inhomogeneous nature of the turbulence level inside an in-line HSM should be taken into well consideration in the process design, optimization and scale-up.

Acknowledgments

This work is financially supported by NSFC (20836005, 21076144) and the Special Funds for Major State Basic Research Program of China (2012CB720300). The authors gratefully acknowledge FLUKO Equipment Shanghai Co. Ltd., for providing the custom-built in-line high shear mixer and offering technical support. Mr. Yao Zhang from Marktec Technology Limited is appreciated for modifications and calibrations of the LDA system as well as discussions on the experimentations.

Notation

C_S = Smagorinsky constant
D = outer swept diameter of the rotor, m
k = turbulent kinetic energy, m^2/s^2
k_1 = power consumption model constant
$LESIQ_v$ = index of LES quality
N = rotational speed, s^{-1}
P_{fluid} = net power input delivered to fluid, W
$Po_{z(t)}$ = turbulent power number at zero flow rate
Q = volumetric flow rate, m^3/s
r = radial coordinate, m
$|S|$ = shear rate at the resolved scale, s^{-1}
T = torque, N m
Tr = period of revolution, s
u = fluid velocity, m/s
u' = velocity fluctuation in the x direction, m/s
V = volume, m^3
$<Vr>$ = ensemble-averaged radial velocity, m/s
$<Vt>$ = ensemble-averaged tangential velocity, m/s
V_{tip} = rotor tip speed (based on the outer swept rotor diameter), m/s
v' = velocity fluctuation in the y direction, m/s
w' = velocity fluctuation in the z direction, m/s
z = axial coordinate, m

Greek letters

Δ = filter width, m
Δt = time step size, s
Δx = length interval, m
ε = turbulent dissipation rate, m^2/s^3
μ = fluid viscosity, Pa s
ν = kinematics viscosity, m^2/s
ν_t = turbulent viscosity, m^2/s
θ = angular coordinate, °
ρ = fluid density, kg/m^3

Subscripts

max = maximum values
res = resolved scale
sgs = subgrid scale
tot = total

Dimensional groups

$Fl = \frac{Q}{ND^3}$ = flow number
$Po = \frac{P_{fluid}}{\rho N^3 D^5}$ = power number
$\mathrm{Re} = \frac{\rho N D^2}{\mu}$ = Reynolds number

Literature Cited

1. Atiemo-Obeng VA, Calabrese RV. Rotor-stator mixing devices. In: Paul EL, Atiemo-Obeng VA, Kresta SM, editors. *Handbook of Industrial Mixing: Science and Practice*. New Jersey: Wiley, 2004: 479–505.
2. Gingras J-P, Tanguy PA, Mariotti S, Chaverot P. Effect of process parameters on bitumen emulsions. *Chem Eng Process*. 2005;44:979–986.
3. Baldyga J, Orciuch W, Makowski L, Malik K, Özcan-Taşkin G, Eagles W, Padron G. Dispersion of nanoparticle clusters in a rotor-stator mixer. *Ind Eng Chem Res*. 2008;47:3652–3663.
4. Özcan-Taşkin NG, Padron G, Voelkel A. Effect of particle type on the mechanisms of break up of nanoscale particle clusters. *Chem Eng Res Des*. 2009;87:468–473.
5. Hassan A, Hassan A. High shear process for producing micronized waxes. US 20100125157A1. H.R.D. Corporation, May 20, 2010.
6. Hall S, Cooke M, El-Hamouz A, Kowalski AJ. Droplet break-up by in-line Silverson rotor–stator mixer. *Chem Eng Sci*. 2011;66:2068–2079.
7. Patterson GK, Paul EL, Kresta SM, Etchells AW. Mixing and chemical reactions. In: Paul EL, Atiemo-Obeng VA, Kresta SM, editors. *Handbook of Industrial Mixing: Science and Practice*. New Jersey: Wiley, 2004:755–867.
8. Bourne JR, Garcia-Rosas J. Rotor-stator mixers for rapid micromixing. *Chem Eng Res Des*. 1986;64:11–17.
9. Bourne JR, Studer M. Fast reactions in rotor-stator mixers of different size. *Chem Eng Process*. 1992;31:285–296.
10. Zhang J, Xu S, Li W. High shear mixers: a review of typical applications and studies on power draw, flow pattern, energy dissipation and transfer properties. *Chem Eng Process*. 2012;57–58:25–41.
11. Calabrese RV, Francis MK, Kevala KR, Mishra VP, Padron GA, Phongikaroon S. Fluid dynamics and emulsification in high shear mixers. *Proceedings of the 3rd World Congress on Emulsions*. Lyon, France, September 24–27, 2002.
12. Xu S, Shi J, Cheng Q, Li W, Zhang J. Residence time distributions of in-line high shear mixers with ultrafine teeth. *Chem Eng Sci*. 2013;87:111–121.
13. Hassan A, Bagherzadeh E, Anthony RG, Borsinger G, Hassan A. System and process for the production of aniline and toluenediamine. US 007750188B2. H.R.D. Corporation, July 6, 2010.
14. Hassan A, Bagherzadeh E, Anthony RG, Borsinger G, Hassan A. High shear system for the production of chlorobenzene. US 20100183486A1. H.R.D. Corporation, July 22, 2010.
15. Hassan A, Bagherzadeh E, Anthony RG, Borsinger G, Hassan A. System for making linear alkylbenzenes. US 20100266465A1. H.R.D. Corporation, October 21, 2010.
16. Hassan A, Bagherzadeh E, Anthony RG, Borsinger G, Hassan A. System and process for production of toluene diisocyanate. US 20110027147A1. H.R.D. Corporation, February 3, 2011.
17. Wei C, Yang B-S. Crystallization via high-shear transformation. US 20060160841A1. Louis J. Wille Bristol-Myers Squibb Company, July 20, 2006.
18. Lee FP-H, Wong RW-N, Kao SV. Process for preparing phase change inks. US 20070030322A1. Xerox Corporation, February 8, 2007.
19. Burris MV, Burris BB, Ajideh H, Clayton A. Methods and systems for manufacturing modified asphalts. US 20090312872 A1. Asphalt Technology LLC, December 17, 2009.
20. Larke CW. High shear process for making metallic esters. US 20050272945 A1. Dover Chemical Corporation, December 8, 2005.
21. Pacek AW, Baker M, Utomo AT. Characterisation of flow pattern in a rotor stator high shear mixer. *Proceedings of the 6th European Congress on Chemical Engineering (ECCE-6)*, Copenhagen, September 16–20, 2007.
22. Utomo AT, Baker M, Pacek AW. Flow pattern, periodicity and energy dissipation in a batch rotor-stator mixer. *Chem Eng Res Des*. 2008;86:1397–1409.
23. Mortensen HH, Calabrese RV, Innings F, Rosendahl L. Characteristics of batch rotor-stator mixer performance elucidated by shaft torque and angle resolved PIV measurements. *Can J Chem Eng*. 2011; 89:1076–1095.
24. Utomo AT, Baker M, Pacek AW. The effect of stator geometry on the flow pattern and energy dissipation rate in a rotor-stator mixer. *Chem Eng Res Des*. 2009;87:533–542.
25. Singh H, Fletcher DF, Nijdam JJ. An assessment of different turbulence models for predicting flow in a baffled tank stirred with a Rushton turbine. *Chem Eng Sci*. 2011;66:5976–5988.
26. Fluent Inc. User's Manual to Fluent 6.3. Fluent Inc.: Lebanon, 2006.
27. Hartmann H, Derksen JJ, Montavon C, Pearson J, Hamill IS, Van den Akker HEA. Assessment of large eddy and RANS stirred tank simulations by means of LDA. *Chem Eng Sci*. 2004;59:2419–2432.
28. Yeoh SL, Papadakis G, Yianneskis M. Numerical simulation of turbulent flow characteristics in a stirred vessel using the LES and RANS approaches with the sliding/deforming mesh methodology. *Chem Eng Res Des*. 2004;82:834–848.
29. Derksen J, Van den Akker HEA. Large eddy simulation on the flow driven by a Rushton turbine. *AIChE J*. 1999;45:209–221.
30. Alcamo R, Micale G, Grisafi F, Brucato A, Ciofalo M. Large-eddy simulation of turbulent flow in an unbaffled stirred tank driven by a Rushton turbine. *Chem Eng Sci*. 2005;60:2303–2316.
31. Hartmann H, Derksen JJ, Van den Akker HEA. Macroinstability uncovered in a Rushton turbine stirred tank by means of LES. *AIChE J*. 2004;50:2383–2393.
32. Yeoh SL, Papadakis G, Yianneskis M. Determination of mixing time and degree of homogeneity in stirred vessels with large eddy simulation. *Chem Eng Sci*. 2005;60:2293–2302.
33. Murthy B, Joshi J. Assessment of standard k-ε, RSM and LES turbulence models in a baffled stirred vessel agitated by various impeller designs. *Chem Eng Sci*. 2008;63:5468–5495.
34. Kato C, Mukai H, Manabe A. Large-eddy simulation of unsteady flow in a mixed-flow pump. *Int J Rotating Mach*. 2003;9:345–351.
35. Sinha M, Katz J, Meneveau C. Quantitative visualization of the flow in a centrifugal pump with diffuser vanes—II: addressing passage-averaged and large-eddy simulation modeling issues in turbomachinery flows. *J Fluids Eng*. 2000;122:108–116.
36. Byskov RK, Jacobsen CB, Pedersen N. Flow in a centrifugal pump impeller at design and off-design conditions-Part II: large eddy simulations. *J Fluids Eng*. 2003;125:73–83.
37. Tokyay TE, Constantinescu SG. Validation of a large-eddy simulation model to simulate flow in pump intakes of realistic geometry. *J Hydraul Eng*. 2006;132:1303–1315.
38. Slack MD, Prasad RO, Bakker A, Boysan F. Advances in cyclone modeling using unstructured grids. *Chem Eng Res Des*. 2000;78: 1098–1104.
39. Delgadillo J, Rajamani R. A comparative study of three turbulence-closure models for the hydrocyclone problem. *Int J Miner Process*. 2005;77:217–230.
40. Brennan M. CFD simulations of hydrocyclones with an air core: comparison between large eddy simulations and a second moment closure. *Chem Eng Res Des*. 2006;84:495–505.
41. Narasimha M, Brennan M, Holtham P. Large eddy simulation of hydrocyclone-prediction of air-core diameter and shape. *Int J Miner Process*. 2006;80:1–14.

42. Kowalski AJ, Cooke M, Hall S. Expression for turbulent power draw of an in-line Silverson high shear mixer. *Chem Eng Sci*. 2011; 66:241–249.
43. Cooke M, Rodgers TL, Kowalski AJ. Power consumption characteristics of an in-line Silverson high shear mixer. *AlChE J*. 2012;58: 1683–1692.
44. Sparks T. Fluid mixing in rotor-stator mixers. Ph.D. Dissertation. Cranfield, Bedfordshire: Cranfield University, 1996.
45. Kowalski A. An expression for the power consumption of in-line rotor-stator devices. *Chem Eng Process*. 2009;48:581–585.
46. Özcan-Taşkin NG, Kubicki D, Padron G. Power and flow characteristics of three rotor-stator heads. *Can J Chem Eng*. 2011;89:1005–1017.
47. Hall S, Cooke M, Pacek AW, Kowalski AJ, Rothman D. Scaling up of Silverson rotor-stator mixers. *Can J Chem Eng*. 2011;89:1040–1050.
48. Launder BE, Spalding DB. *Lectures in Mathematical Models of Turbulence*. London: Academic Press, 1972.
49. Sheng J, Meng H, Fox RO. A large eddy PIV method for turbulence dissipation rate estimation. *Chem Eng Sci*. 2000;55:4423–4434.
50. Sagaut P. *Large Eddy Simulation for Incompressible Flows*. Berlin Heidelberg: Springer, 2006.
51. Meyers J, Geurts BJ, Sagaut P. *Quality and Reliability of Large-Eddy Simulations*. ERCOFTAC Series, Vol. 12. Berlin Heidelberg: Springer, 2008.
52. Lee KC, Yianneskis M. Turbulence properties of the impeller stream of a Rushton turbine. *AlChE J*. 1998;44:13–24.
53. Li Z, Bao Y, Gao Z. PIV experiments and large eddy simulations of single-loop flow fields in Rushton turbine stirred tanks. *Chem Eng Sci*. 2011;66:1219–1231.
54. Barailler F, Heniche M, Tanguy P. CFD analysis of a rotor-stator mixer with viscous fluids. *Chem Eng Sci*. 2006;61:2888–2894.
55. Cheng Q, Xu S, Shi J, Li W, Zhang J. Pump capacity and power consumption of two commercial in-line high shear mixers. *Ind Eng Chem Res*. 2013;52:525–537.

Manuscript received Dec. 3, 2012, and revision received Nov. 18, 2013.